ISSN : 2455-9679
Impact Factor : 2.865


IJRTSM

INTERNATIONAL JOURNAL OF RECENT TECHNOLOGY SCIENCE & MANAGEMENT

# "EXCEPTIONALLY SCATTERED NICKEL NANOPARTICLES ADORNED TITANIUM DIOXIDE NANOTUBE EXHIBIT FOR IMPROVED SUN ORIENTED LIGHT INGESTION"

***Mrs. Vaishali Gupta*** [1], ***Dr. Brajesh Dixit*** [2], ***Dr Deepesh Kumar Dixit*** [3]

[1] *Phd Scholar , Department of Physics, P.K. University, Shivpuri, MP, India*

[2] *Associate Professor, SR group of institution Jhansi,UP, India*

[3] *Associate Professor, Shrimati Omvati College, Kotra, Jalaun,UP, India*

## ABSTRACT

***Honeycomb titanium dioxide nanotube exhibit (TiO2-NTA) adorned by profoundly scattered nickel nanoparticles (Ni-NPs) has been developed leveled out on Ti foil by anodization and ensuing electrodeposition. The pore distance across and length of TiO2-NTA, and the size and amount of Ni-NPs can be controlled through regulating the factors of the electrochemical cycles. It has been tracked down that the pretreatment of TiO2-NTA in the Cu(NO3)2 arrangement and further toughening at 450 °C in air could enormously improve the scattering of the electrodeposited Ni- NPs. Ingestion of the light in the sunlight based range from 300 to 2500 nm by the Ni-NPs@TiO2-NTA is just about as high as 96.83%, on account of the co-impact of the light-catching of TiO2-NTA and the plasmonic reverberation of Ni-NPs. In the water warming analysis performed under an enlightening sun oriented force thickness of ∼1 kWm−2 (AM 1.5), the extreme temperature more than 66 °C and a general productivity of 78.9% inside 30 min were gotten, promising for applications in photo thermal transformation and sun powered energy reap.***

***Key Words:*** *Honeycomb ,Titanium dioxide nanotube exhibit, (TiO2-NTA), Ni-NPs*

## I. INTRODUCTION

Photograph warm transformation, the immediate method of sun based use, is one of the critical strategies to gather sun oriented energy and has been generally examined in, for instance, water steam age [1–5], desalination [6–8], sun powered nuclear energy age [9,10], sun powered thermoelectric change [11,12], and sun powered fuel creation [13]. A profoundly productive safeguard is the vital piece of a sun oriented assortment framework, which ingests sunlight based energy, changes over it straightforwardly to nuclear power which is then consumed by a warmth move liquid. As of now, there are three kinds of standard photo thermal change materials that have been proposed and considered, counting the carbon-based materials, metallic plasmonic materials and semiconducting materials [14–16].

Up to now, different metal nanoparticles (e.g., Au-NPs [15], Ag-NPs [17], Al-NPs [6,18] and In- NPs [7]) have been discovered great for light ingestion and photo thermal transformation dependent on a superficial level plasmonic reverberation, an aggregate wavering of free electrons in the metal invigorated by photons with the coordinating with recurrence [19]. By and by, there are a few hindrances to huge scope applications. For example, Au and Ag are honorable metals, prompting a significant expense, while Al-NPs and In-NPs with moderately high synthetic action are normally set up by a complex measure, including vacuum affidavit. In Ni-NPs, the advances of sp-electrons and incompletely filled d-groups (3d8) add to upgraded retention in a more extensive otherworldly district [20–22], which is wanted for collecting sun based energy [23,24]. Despite the fact that their light retention ability is more vulnerable

ISSN : 2455-9679
Impact Factor : 2.865

than honorable metal nanoparticles, Ni-NPs are a promising elective for light retention because of their minimal effort just as plausible and effortless amalgamation by different techniques, including synthetic decrease and electrodeposition [25,26]. TiO2, a broadly considered semiconductor with a wide band hole of ~3.2 eV, just reacts to the bright (7% of complete range) and is generally filled in as the network or backing in engrossing materials attributable to the great steadiness, for example, C-TiO2 [27], CNT-TiO2 [28] and Au-TiO2 [29], where different unpleasant or permeable surface constructions are intended to improve retention by smothering the surface reflection. As of late,miniature/nano- permeable constructions with solid light assimilation have been intended for sunlight based gathering because of the improved light-catching impact of the mathematical interspace, where light goes through numerous reflections what's more, dissipating inside, and is retained slowly [30,31]. For instance, a super low reflectance of 0.045% was accomplished on vertical carbon nanotube exhibits [32]. Plus, a progression of raised miniature nano structures have been in situ manufactured by laser composing on Si [33], copper [34], titanium and tungsten surfaces [35], which all display reflectance beneath 2.5%. For example, a new report exhibited that the wedge-formed TiO2 cluster could retain light in the entire sun oriented range [36]. In this, we report the manufacture of the honeycomb-formed TiO2- NTA brightened with Ni-NPs on Ti foil by anodization and resulting electrodeposition. The permeable TiO2-NTA not just give the design for light-catching yet additionally work as the help for 3-D dispersed plasmonic Ni-NPs. The creation cycle is delineated in Fig. 1. Curiously, Ni-NPs have been found to consistently store on the TiO2- NTA and the streamlined Ni-NPs@TiO2-NTA half and half shows a solid assimilation in the sun based range of 0.3–2.5 μm, affirming the potential utilization of this remarkable half breed for collecting sun oriented energy.

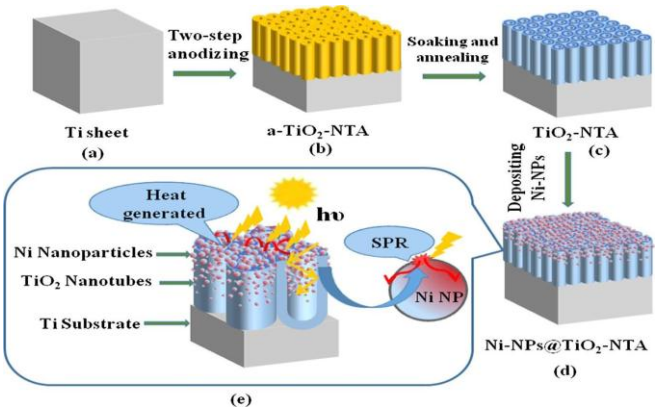


Fig. 1. Synthesis procedure for the Ni-NPs@TiO2-NTA: (a) the original Ti sheet, (b) a-TiO2-NTA fabricated by a two-step anodizing, (c) the Cu(NO3)2 solution soaked and annealed TiO2-NTA, (d) the electrochemically deposited Ni-NPs on TiO2-NTA, (e) the enlarged part of (d), showing the photo thermal conversion mechanisms.

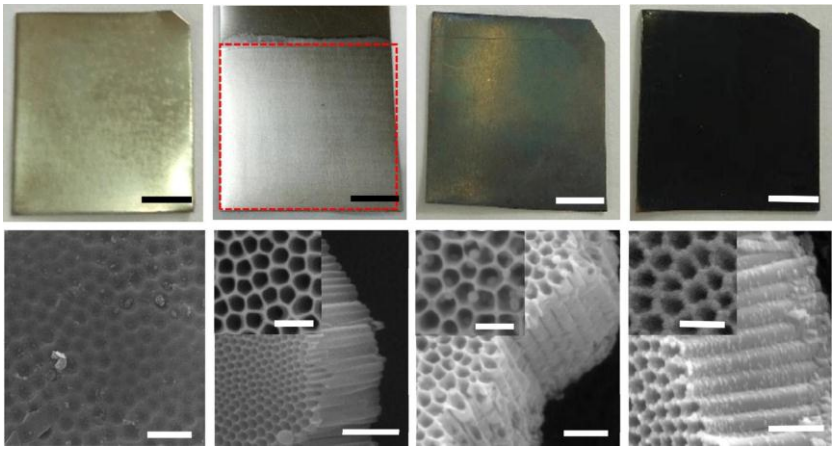

Fig. 2. Optical photographs: (a) Ti sheet, (b) Ti sheet after removing the first-anodized film, (c) Annealed TiO2- NTA, and (d) Ni-NPs@TiO2-NTA. SEM images: (e) The pre-patterned Ti sheet, (f) TiO2-NTA, (g) Ni-NPs@TiO2- NTA without soaking and (h) Ni-NPs@TiO2-NTA with soaking in the Cu(NO3)2 solution. The inserts in (f), (g) and (h) are the corresponding enlarged top views.

ISSN : 2455-9679
Impact Factor : 2.865

## II. EXPERIMENTAL WORK

### 2.1. Preparation of TiO2-NTA

Ti sheets (99.5% immaculateness) were cut into wanted sizes (for example 50×33×0.2mm3), cleaned from coarse to fine on sand papers, ultrasonically cleaned in ethanol and dried in air. Glue tapes were to utilized cover the rear of the Ti sheet with the goal that just one side of the sheet with a territory of 10 cm2 was presented to the electrolyte. Exceptionally uniform furthermore, requested undefined TiO2-NTA (a-TiO2-NTA) were created by a two-venture anodization measure [37]. All the anodization tests were done at 25 °C in a traditional two-cathode cell with graphite as the cathode. The initial step was performed at 20, 40, 60, 80 V for 0.5 hr in the ethylene glycol electrolyte containing 0.7 wt% NH4F, 6 vol% H2O and 4 vol% H3PO4. The first-anodized a-TiO2-NTA were washed in deionized water and the anodized film was taken off utilizing a sticky tape to uncover the pre-designed Ti substrate. The second-step anodization was acted in the indistinguishable electrolyte for 10–70 min, what's more, the voltage was generally 20 V higher than the relating firststep. The examples were then washed in ethanol to eliminate the remaining electrolyte and the sticky tape was taken out from the rear of the anodized Ti sheet. Consequently, the anodized Ti sheets were doused into a 0.05 Cu(NO3)2·3H2O ethanol answer for 6 hr and strengthened in air at 450 °C for 3 hr.

### 2.2. Readiness of Ni-NPs@TiO2-NTA

The Ni-NPs were kept on the divider and surface of the TiO2-NTA by electrodeposition under a steady current in a two-cathode cell containing 0.3M NiSO4·7H2O, 0.3M H3BO3 and 0.1 g L−1 lauryl sodium sulfate. In this cell, the cathode was the tempered Ti sheet, and the anode was graphite. The electrodeposition was completed at 35 °C under a high current thickness of 30 mA cm−1 for 0–100 s. At last, the gotten dark examples were washed in water, and dried at 80 °C in air.

### 2.3. Portrayal of materials

The morphology of Ni-NPs@TiO2-NTA on the Ti substrate was portrayed with an examining electron magnifying lens (SEM, PHILPS XL30TMP). The stage structures of the examples were recorded by a X-beam diffractometer (XRD, Xpert Pro MPD). Optical properties (reflectance what's more, absorptance) and band hole were estimated by an UV–Vis what's more, NIR spectrophotometer (Shimadzu 3600 UV/Vis and Shimadzu 2600 UV/Vis) consolidated with a coordinating circle. The in general warm efficiencies of tests were explored utilizing an in-house planned water warming cell under the radiation (AM 1.5) of a sun powered test system (LSP- X500A). The mimicked daylight lighted on the Ni- NPs@TiO2-NTA side of the Ti sheet whose posterior shaped a piece of the mass of the water warming cell containing 8.5 mL water.

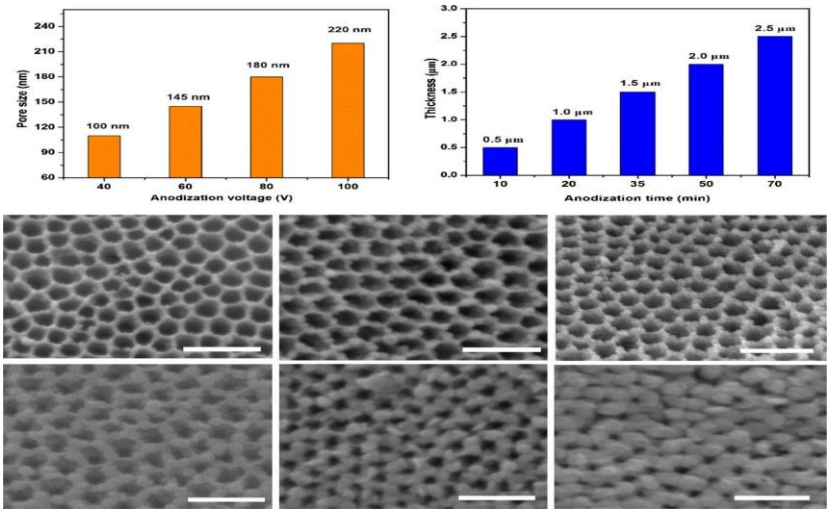


Fig. 3. (a) The average pore size of TiO2-NTA under different anodization voltages. (b) The average thickness of TiO2-NTA anodized at 60 V with various anodization times. SEM images of Ni-NPs@TiO2-NTA with different deposition times: (c) 6.25 s, (d) 12.5 s, (e) 25 s, (f) 50 s, (g) 75 s, (h), 100 s. The TiO2-NTA in (c) and (h) were anodized at 60 V for 50 min

ISSN : 2455-9679
Impact Factor : 2.865

## III. RESULTS AND DISCUSSION

### 3.1 Morphologies and structures

The computerized photos appeared in Fig. 2 were taken from the surfaces of the Ti sheet toward the finish of each progression of cleaning and cleaning (Fig. 2a), eliminating the primary anodized film (Fig. 2b), drenching and toughening (Fig. 2c), and storing Ni-NPs (Fig. 2d). As demonstrated in Fig. 2b–d, the continuous obscuring of the example shows that light assimilation would be improved seriatim. Normal SEM pictures of different tests are shown in Fig. 2e–h. The pre- designed Ti substrate after utilizing sticky tape to eliminate the principal anodized film was appeared in Fig. 2e. The uniform TiO2 NTA tests with an mass of unit cells with measurement of 150–200 nm were developed after the two-venture anodization (Fig. 2f). In the wake of tempering and consistent current keeping, the meager Ni-NPs with a normal width of ~65 nm were kept on the internal mass of each TiO2-NTA (Fig. 2g). Nonetheless, when the TiO2 NTAs were absorbed the weaken Cu(NO3)2 arrangement prior to strengthening, the thickly loaded Ni-NPs with clear shape profiles and diminished normal breadth of ~40 nm were consistently stored on both the top furthermore, mass of each TiO2-NTA (Fig. 2h). Besides, contrasted with the detailed works [38,39], the as-arranged Ni-NPs are more modest in size and profoundly circulated on each TiO2- NTA, which shows that the splashing treatment assumed a critical part in the development of Ni- NPs. In addition, we saw that when electrodeposition was done straightforwardly of the strengthened Ti sheet without the TiO2-NTA covering, the kept Ni shaped a consistent, smooth, and thick shimmering covering. This change is especially not quite the same as the granular and dark Ni-NPs on the TiO2-NTA. The reason might be that the higher obstruction of the TiO2-NTA diminished the development rate and the last size of Ni-NPs [40], and the permeable TiO2-NTA offered more 3-D testimony destinations for Ni-NPs to frustrate the get-together of Ni-NPs [41]. The morphological highlights of Ni-NPs@TiO2-NTA, for example, pore size, thickness (or the length of the nanotubes) and molecule size and sum of Ni-NPs, are the determinants for light retention, which were examined by finely controlling the electrochemical boundaries. The outline appeared in Fig. 3a shows that the pore size of TiO2-NTA increments with the anodization voltage because of the upgraded electric field [42]. As demonstrated in Fig. 3b, the thickness of TiO2- NTA likewise increments with the anodization time, however the development speed is easing back down. In Fig. 3c–h, the normal molecule sizes of Ni-NPs with various affidavit times are around 20, 30, 40, 60, 100 and 150 nm, separately. It is clear that the molecule size and measure of Ni-NPs increment ceaselessly as affidavit time increments. Subsequently, the excess pore size bit by bit contracts and vanishes at last. The XRD examples of as-arranged and heat treated Ni-NPs@TiO2- NTAs are appeared in Fig. 4a. The fundamental elements of the example dried at 80
°C are affirmed to be anatase-TiO2 by the diffraction tops at 25.3°, 37.8°, 48.0°, 53.9° and 55.0° (JCPDF No. 21-1272), metallic Ni at 44.5° also, 76.4° (JCPDF No. 04-8050). The diffraction tops at 35.1°, 38.4°, 40.2°, 53.0°, 62.9° and 70.6° have a place with the substrate Ti (JCPDF No. 44- 1294). There were no obvious diffraction pinnacles of NiO in the XRD designs in the event that the example was warmed at temperatures lower than 250 °C, showing that the metallic Ni is steady in air under 250 °C. At the point when the temperature rose to 300 °C and 350 °C, the evident diffraction top at 43.2° for NiO (JCPDF No. 47-1049), just as the augmented width Ni-NPs appeared in Fig. 4b show that the Ni-NPs were oxidized and changed to NiO. In later analyses, the Ni-NPs@TiO2-NTA were warmed at 500 °C for 5 h in a diminishing climate containing 5% hydrogen. As demonstrated in Fig. 4c, in the diminishing climate, the Ni-NPs kept on side mass of TiO2-NTA grew up because of the blend of more modest particles at high temperatures, while

ISSN : 2455-9679
Impact Factor : 2.865

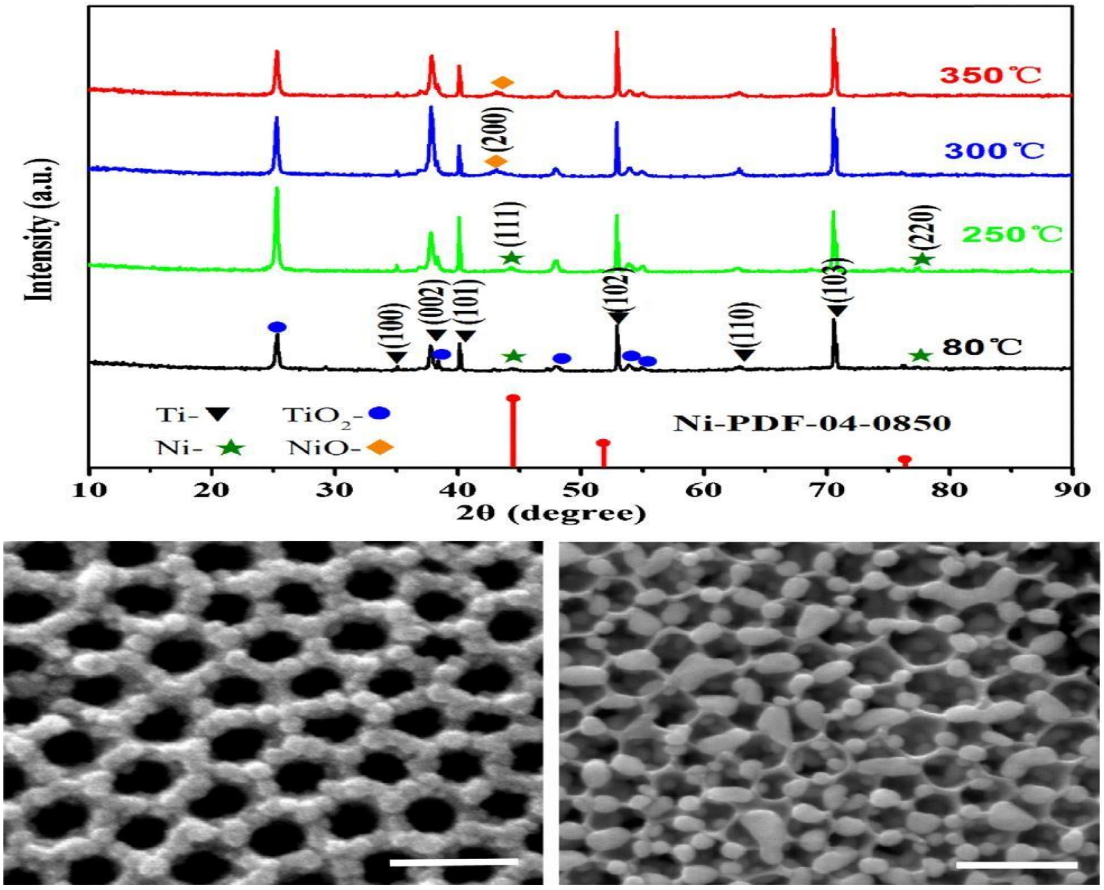


Fig. 4. (a) XRD patterns of Ni-NPs@TiO2-NTA treated in air at different temperatures.
(b) SEM image of Ni-NPs@TiO2-NTA treated at 350 °C. (c) SEM image of Ni-NPs@TiO2-NTA treated in H2/Ar.

### 3.1. Light absorption

The light assimilation capacities of the Ni-NPs@TiO2-NTA tests were estimated through spectrophotometers with a coordinating circle and assessed by absorptance and reflectance. The weighted sun oriented absorptance (α) was determined by the deliberate reflection range what's more, standard sun based radiation range by the accompanying conditions [43]:

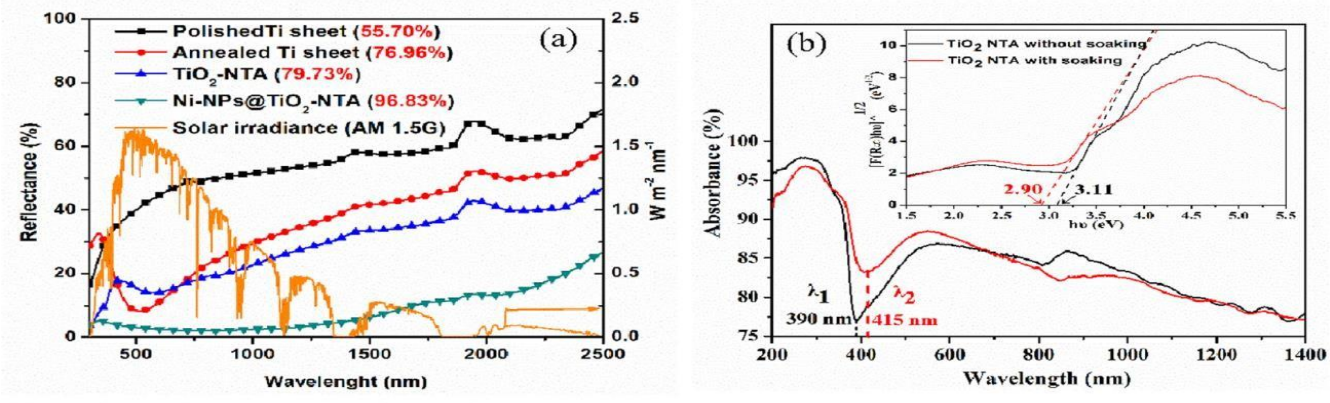


Fig. 5. (a) Solar radiation spectrum and reflection spectra for different surfaces on Ti substrates. (b) Absorptance spectra and Kubelka–Munk plot (the insert) of TiO2-NTA with and without soaking.

ISSN : 2455-9679
Impact Factor : 2.865

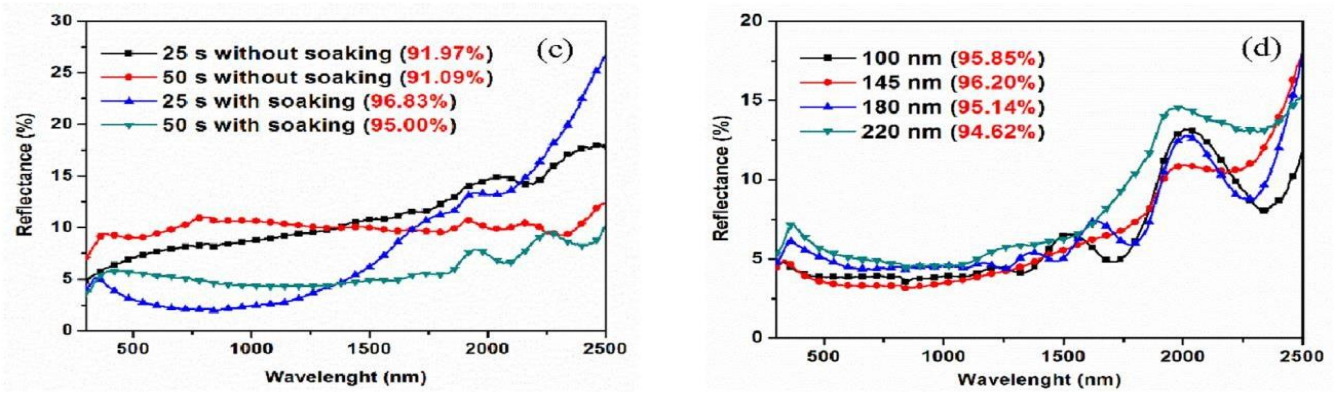


Fig 5. (c) Reflection spectra for Ni- NPs@TiO2-NTA with and without soaking. (d) Reflection spectra for Ni-NPs@TiO2-NTA with a thickness of 2 μm and different pore sizes.

The data in bracket is the weighted absorptance of the samples. where λ is the frequency, R(λ) is the reflectance of per unit frequency for the manufactured examples. Isol(λ) is the sun based radiation power of per unit frequency, accroding to the ISO standard 9845-1(1992) of AM 1.5. The band hole (or energy hole) of the diverse TiO2 tests was determined by the Kubelka-Munk condition of F(R)=(1−R)2/(2R), where R is the reflectance comparative with BaSO4 [44]. As demonstrated in Fig. 5a, the cleaned Ti sheet showed the most elevated reflectance on account of the all around cleaned surface and inherent low assimilation of metallic Ti. Contrasted with the reduced TiO2 film on toughened Ti, the absorptance of TiO2- NTA further expanded as the permeable surface caught all the more light. The least reflectance was seen on the Ni- NPs@TiO2-NTA test because of the serious extra assimilation of Ni-NPs dependent on plasma reverberation, which is a notable impact of metal nanoparticles. Despite the fact that it has been accounted for that CuO nanoparticles likewise display the retention, dispersing and plasmon impact in the sunlight based range [45], the low substance (~0.56 at% Cu from EDS yet undetectable in SEM pictures) and the front of Ni-NPs may prompt close to nothing ingestion through CuO itself. As demonstrated in Fig. 5b, the assimilation cutoff frequency (λ1 and λ2) of the TiO2-NTA without and with splashing is individually ~390 nm and 415 nm, and the TiO2-

NTA with splashing displays more grounded ingestion in the obvious light district, yet more fragile in the bright district. The conceivable explanation is that the CuO with a thin band hole of ~1.7 eV has a solid ingestion limit in the obvious district and may diminish the assimilation of the TiO2- NTA in the bright district because of the protecting impact. The Kubelka–Munk plots in the addition of Fig. 5b show the band holes of 3.11 and 2.90 eV of the unsoaked and doused tests, and the diminished bandgap of the last might be begun from the Cu2+ doping of the substrate [46]

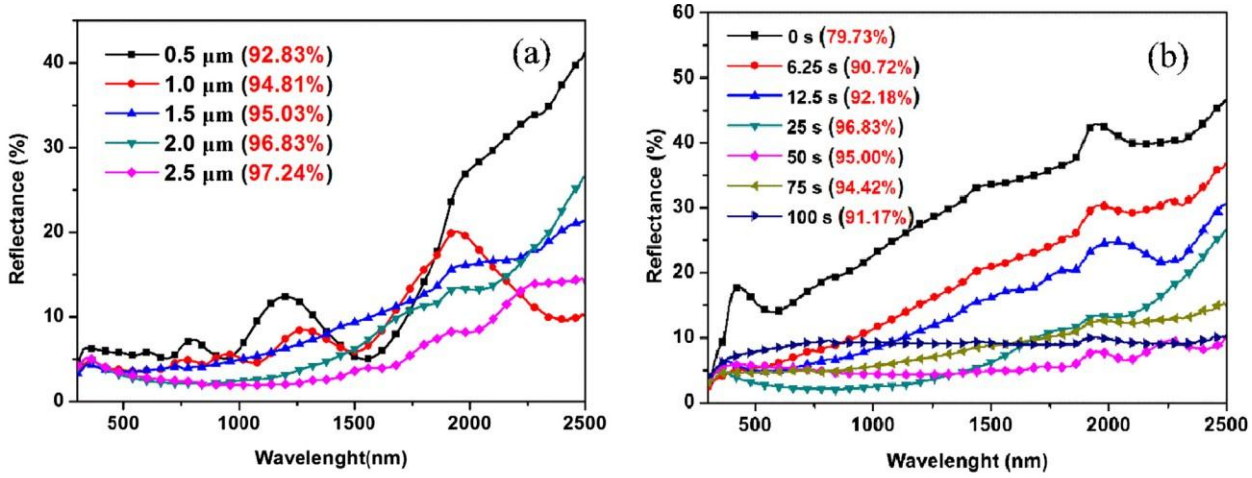


Fig. 6. (a) Reflection spectra for Ni-NPs@TiO2-NTA with different thicknesses. (b) Reflection spectra for Ni-NPs@TiO2-NTA with different Ni deposition times.

ISSN : 2455-9679
Impact Factor : 2.865

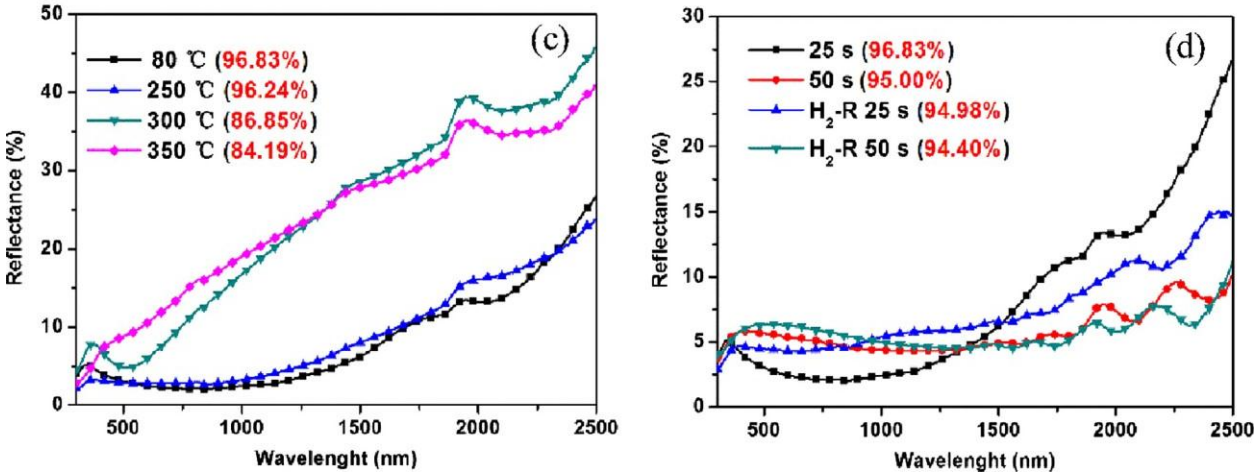


Fig. 6 (c) Reflection spectra for Ni-NPs@TiO2-NTA with different calcination temperatures. (d) Reflection spectra for Ni-NPs@TiO2-NTA with H2 reduction.

Contrasted with the unsoaked test, the retention of the Ni-saved TiO2-NTA with dousing is expanded by ~5% (Fig. 5c), and the sum of the Ni-NPs is expanded and the size is diminished (Fig. 2g and h), showing that a little amount of CuO came about because of the decomposion of the ingested Cu(NO3)2 may upgrade the retention of Ni- NPs@TiO2-NTA by balancing the nucleation and changing the morphology of the Ni-NPs [47]. Besides, the serious development of between various Ni-NPs may limit themselves to become bigger inside the minute space of the TiO2 nanotubes where electrolyte and Ni2+ supply was restricted. Thus, the Ni-NPs with more modest size (~40 nm) and very much disseminated on the TiO2-NTA, showed more grounded light ingestion in the band of 300–1200 nm, however a lower retention in the center to far infrared districts, which can be attributed to the size dependent reverberation hypothesis that the most extreme assimilation locale of plasmonic metal particles relies upon their size and shape, and the retention band red movements with the increment of molecule size and angle proportion [48–51]. Incidentally, ingestion district shifts with the size of Ni- NPs, in this manner the a lot of Ni-NPs with shifting sizes could show a expansive light retention locale. Fig. 5d shows the reflection spectra for the Ni-NPs@TiO2-NTA with various pore sizes. It very well may be seen that the retention locale and by and large absorptance are roughly equivalent, showing that the retention for Ni-NPs@TiO2-NTA isn't delicate to the pore size. Albeit a bigger TiO2 nanotube can oblige more Ni-NPs and catch all the more light for a solitary nanotube, the entire surface territory and measure of stacked Ni-NPs are contrarily relative to the width of the pore. Accordingly, the Ni- NPs@TiO2-NTA anodized at 60 V with the suitable pore size of ~145 nm showed the most elevated absorptance. The impact of the Ni-NPs@TiO2-NTA thickness on light assimilation is exhibited in Fig. 6a. Right off the bat, particular vacillations can be seen in the reflection spectra for Ni-NPs@TiO2-NTA with thickness of 0.5 what's more, 1.0 μm, which can be credited to the damaging and valuable obstructions [52,53]. Likewise, the general absorptance increments with the thickness because of more careful retention in the more extended optical way. In particular, as the coatings became thicker, more Ni-NPs were kept on the inward dividers and more reflection and dispersing happened in the cylinders, adding to higher absorptance. Albeit the absorptance of the 2.5 μm thick covering was up to 97.24%, the covering would pleat and separate from the Ti substrate effectively, likely in light of the fact that development in thick Ni-NPs@TiO2-NTA was likely lopsided, and consequently cause restricted pressure advancement. In this way, an ideal thickness of 2 μm was set in the resulting tests. As demonstrated in Fig. 6b, the reflection spectra are appeared for a progression of Ni-NPs@TiO2-NTA anodized at 60 V for 50 min followed by electrodeposition at different occasions. With the augmentation of statement time (less than 25 s), the sum and size of Ni-NPs expanded bit by bit, due to the satisfactory nucleation and development of the particles. The entire band absorptance expanded with the increment of the quantity of Ni- NPs. The Ni-NPs@TiO2-NTA acquired from statement for 25 s showed the most noteworthy absorptance of noticeable light and a greatest entire range absorptance of 96.83%, which is near to that of the revealed materials with comparative permeable constructions, for example, the Al- NPs@Al2O3- NTA (~96%), Au@Al2O3 (91%) and the Ni particles pigmented anodized aluminum (94–96%)

ISSN : 2455-9679
Impact Factor : 2.865

[4,29,54]. Nonetheless, when the affidavit time was additionally delayed (in excess of 25 s), the kept Ni-NPs developed adequately large to fill the pores. The pore size continuously diminished with the ceaseless statement of Ni particles, and all the more light was reflected off the surface, instead of enter the nanotubes, prompting the decay of absorptance particularly for the obvious light (the shade of the test changed over to yellow and white). The Ni- NPs@TiO2-NTA tests were further thermally treated at various temperatures and airs. As demonstrated in Fig. 6c, the absorptance didn't decrease when the temperature was lower than 250

°C, yet, essentially decayed at 300 °C, showing that the metallic Ni- NPs with high light retention could stay stable at 250 °C, yet the nickel oxides shaped at higher temperatures carried on inadequately in light retention. Then again, the substances like dark nickel mixtures of NiOOH and Ni2O3 may both exist in the Ni-NPs@TiO2- NTA and add to light ingestion. In later trials, the Ni- NPs@TiO2-NTA were warmed at 500 °C in the decreasing air containing 5% hydrogen. Subsequently, the reflectance as demonstrated in Fig. 6d constricted somewhat in the obvious area and a little upgrade in the infrared locale, most likely because of the development, combination and accumulation of Ni-NPs at 500 °C. In rundown, the high and disintegrated absorptances of Ni- NPs@TiO2-NTA without and with warm oxidation show that the metallic Ni-NPs with an adequate number of free electrons are essential to the high absorptance

## IV. CONCLUSIONS

The Ni-NPs@TiO2-NTA have been combined on the Ti substrate by anodization and electrodeposition. A pretreatment of the TiO2-NTA in the ethanol arrangement of Cu(NO3)2 can essentially scale back the Ni-NPs furthermore, improve light retention by about 5%. The absorptance increments with the thickness of the Ni-NPs@TiO2-NTA, however isn't touchy to the pore size. Besides, the size and measure of Ni-NPs have a critical impact on light retention. Because of the light-catching capacity of the permeable TiO2-NTA and the surface plasmon reverberation of Ni-NPs, a high absorptance of 96.83% in the sun based range from 300 to 2500 nm has been accomplished. In the water warming investigation, the most noteworthy temperature more than 66 °C and a general proficiency of 78.9% inside 30 min light have been acquired, suggesting the likely utilizations of the Ni-NPs@TiO2-NTA in light-to-warm transformation and sun powered energy collect.

## REFERENCES

1. G. Ni, G. Li, S.V. Boriskina, H. Li, W. Yang, T. Zhang, G. Chen, Steam generation under one sun enabled by a floating structure with thermal concentration, Nat.Energy 1 (2016) 16126.
2. K. Bae, G. Kang, S.K. Cho, W. Park, K. Kim, W.J. Padilla, Flexible thin-film black gold membranes with ultrabroadband plasmonic nanofocusing for efficient solar vapour generation, Nat. Commun. 6 (2015) 10103.
3. H.L. Ren, M. Tang, B.L. Guan, K.X. Wang, J.W. Yang, F.F. Wang, M.Z. Wang, J.Y. Shan, Z.L. Chen, D. Wei, H.L. Peng, Z.F. Liu, Hierarchical graphene foam for efficient omnidirectional solar-thermal energy conversion, Adv. Mater. 29 (2017) 1702590.
4. L. Zhou, Y.L. Tan, D.X. Ji, B. Zhu, P. Zhang, J. Xu, Q.Q. Gan, Z.F. Yu, J. Zhu, Selfassembly of highly efficient, broadband plasmonic absorbers for solar steam generation, Sci. Adv. 2 (2016) 1501227.
5. C.J. Chen, Y.J. Li, J.W. Song, Z. Yang, Y.D. Kuang, E. Hitz, C. Jia, A. Gong, F. Jiang, J.Y. Zhu, B. Yang, J. Xie, L.B. Hu, Highly flexible and efficient solar steam generation device, Adv. Mater. 29 (2017) 1701756.
6. L. Zhou, Y. Tan, J. Wang, W. Xu, Y. Yuan, W. Cai, S. Zhu, J. Zhu, 3D self-assembly of aluminium nanoparticles for plasmon-enhanced solar desalination, Nat. Photo. 10 (2016) 393–398.
7. L.L. Zhang, J. Xing, X.L. Wen, J.W. Chai, S.J. Wang, Q.H. Xiong, Plasmonic heating from indium nanoparticles on a floating microporous membrane for enhanced solar seawater desalination, Nanoscale 9 (2017) 12843–12849.
8. M.Y. Shang, N. Li, S.D. Zhang, T.T. Zhao, C. Zhang, C. Liu, H.F. Li, Z.Y. Wang, Fullspectrum solar-to-heat conversion membrane with interfacial plasmonic heating ability for high-efficiency desalination of seawater, ACS Appl. Energy Mater. 1 (2017) 56–61.
9. J.Y. Moon, D.L. Lu, B.V. Saders, T.K. Kim, S.D. Kong, S.H. Jin, R.K. Chen, Z.W. Liu, High performance multi-scaled nanostructured spectrally selective coating for concentrating solar power, Nano Energy 8 (2014) 238–246.

ISSN : 2455-9679
Impact Factor : 2.865


**10.** Q.J. Mao, Recent developments in geometrical configurations of thermal energy storage for concentrating solar power plant, Renew. Sust. Energy Rev. 59 (2016) 320–327.

**11.** L.L. Baranowski, G.J. Snyder, E.S. Toberer, Concentrated solar thermoelectric generators, Energy Environ. Sci. 5 (2012) 9055–9067.

**12.** A. Kosuga, Y. Yamamoto, M. Miyai, M. Matsuzawa, Y. Nishimura, S. Hidaka, K. Yamamoto, S. Tanaka, Y. Yamamoto, S. Tokonami, T. Iida, A high performance photothermal film with spherical shell-type metallic nanocomposites for solar thermoelectric conversion, Nanoscale 7 (2015) 7580–7584.

**13.** X.G. Meng, T. Wang, L.Q. Liu, S.X. Ouyang, P. Li, H.L. Hu, T. Kako, H. Iwai, A. Tanaka, J.H. Ye, Photothermal conversion of CO2 into CH4 with H2 over Group VIII nanocatalysts: an alternative approach for solar fuel production, Angew. Chem. 53 (2014) 11662–11666.

**14.** J.L. Yang, Y.S. Pang, W.X. Huang, S.K. Shaw, J. Schiffbauer, M.A. Pillers, X. Mu, S.R. Luo, T. Zhang, Y.J. Huang, G.X. Li, S. Ptasinska, M. Lieberman, T.F. Luo, Functionalized graphene enables highly efficient solar thermal steam generation, ACS Nano 11 (2017) 5510–5536.

**15.** X.Z. Wang, Y.R. He, X. Liu, G. Cheng, J.Q. Zhu, Solar steam generation through bioinspired interface heating of broadband-absorbing plasmonic membranes, Appl. Energy 195 (2017) 414– 425.

**16.** M.M. Ye, J. Jia, Z.J. Wu, C.X. Qian, R. Chen, P.G. O'Brien, W. Sun, Y.C. Dong, G.A. Ozin, Synthesis of black TiOx nanoparticles by Mg reduction of TiO2 nanocrystals and their application for solar water evaporation, Adv. Energy Mater. 7 (2017) 1601811.

**17.** F. Wu, X.Y. Hu, J. Fan, E.Z. Liu, T. Sun, L.M. Kang, W.Q. Hou, C.J. Zhu, H.C. Liu, Photocatalytic activity of Ag/TiO2 nanotube arrays enhanced by surface plasmon resonance and application in hydrogen evolution by water splitting, Plasmonics 8 (2013) 501–508.

**18.** D.B. Zhang, X.F. Yang, X.K. Hong, Y.S. Liu, J.F. Feng, Aluminum nanoparticles enhanced light absorption in silicon solar cell by surface plasmon resonance, Opt. Quan. Electr. 47 (2014) 1421–1427.

**19.** G. Dodekatos, S. Schunemann, H. Tuysuz, Surface plasmon-assisted solar energy conversion, Top. Cur. Chem. 371 (2015) 215–252.

**20.** S. Zhu, L.M. Wang, Optical and magnetic properties of Ni nanoparticles in rutile formed by Ni ion implantation, Appl. Phys. Lett. 88 (2006).

**21.** V. Dalouji, Effect of deposition time on surface plasmon resonance and Maxwell- Garnett absorption in RF-magnetron sputtered carbon-nickel films, Mater. Sci. Poland 34 (2016) 337–343.

**22.** X. Xiang, X.T. Zu, S. Zhu, L.M. Wang, Optical properties of metallic nanoparticles in Ni-ion-implanted α-Al2O3 single crystals, Appl. Phys. Lett. 84 (2004) 52–54.

**23.** M. Farooq, A.A. Green, M.G. Hutchins, High performance sputtered Ni:SiO2 composite solar absorber surfaces, Sol. Energy Mater. Sol. Cells 54 (1998) 67–73.

**24.** F. Cao, D. Kraemer, T.Y. Sun, Y.C. Lan, G. Chen, Z.F. Ren, Enhanced thermal stability of W-Ni-Al2O3 cermet-based spectrally selective solar absorbers with tungsten infrared reflectors, Adv. Energy Mater. 5 (2015) 1401042.

**25.** L.H. Chou, W.C. Hung, M.T. Lee, On the preparation of nickel nanoparticles by chemical reduction method: X-ray absorption spectroscopy, Mater. Sci. 22 (2016) 305–308.

**26.** Y.H. Zhang, Y.N. Yang, P. Xiao, X.N. Zhang, L. Lu, L. Li, Preparation of Ni nanoparticle- TiO2 nanotube composite by pulse electrodeposition, Mater. Lett. 63 (2009) 2429–2431.

**27.** B. Cheng, K.K. Wang, K.P. Wang, W. Jiang, B.J. Cong, C.L. Song, S.H. Jia, G.R. Han, Y. Liu, Porous carbon-titania nanocomposite films for spectrally solar selective absorbers, Sol. Energy Mater. Sol. Cells 133 (2015) 126–132.

**28.** M.E. Rincón, J.D. Molina, M. Sánchez, C. Arancibia, E. García, Optical characterization of tandem absorber/reflector systems based on titanium oxide-carbon coatings, Sol. Energy Mater. Sol. Cells 91 (2007) 1421–1425.

**29.** E.Z. Liu, J. Fan, X.Y. Hu, Y. Hu, H. Li, C.N. Tang, L. Sun, J. Wan, A facile strategy to fabricate plasmonic Au/TiO2 nano-grass films with overlapping visible light-harvesting structures for H2 production from water, J. Mater. Sci. 50 (2014) 2298–2305.

**30.** Y. Li, Z.Y. Fu, B.L. Su, Hierarchically structured porous materials for energy conversion and storage, Adv. Funct. Mater. 22 (2012) 4634–4667.

ISSN : 2455-9679
Impact Factor : 2.865


**31.** S.K. Yang, N. Sun, B.B. Stogin, J. Wang, Y. Huang, T.S. Wong, Ultra-antireflective synthetic brochosomes, Nat. Commu. 8 (2017) 1285–1293.

**32.** Z.P. Yang, L.J. Ci, J.A. Bur, S.Y. Lin, P.M. Ajayan, Experimental observation of an extremely dark material made by a low-density nanotube array, Nano Lett. 8 (2008) 446–451.

**33.** J. Yang, F.F. Luo, T.S. Kao, X. Li, G.W. Ho, J.H. Teng, X.G. Luo, M.H. Hong, Design and fabrication of broadband ultralow reflectivity black Si surfaces by laser micro/ nanoprocessing, Light: Sci. Appl. 3 (2014) 185.

**34.** P.X. Fan, H. Wu, M.L. Zhong, H.J. Zhang, B.F. Bai, G.F. Jin, Large scale cauliflower shaped hierarchical copper nanostructures for efficient photothermal conversion, Nanoscale 8 (2016) 14617–14624.

**35.** P.X. Fan, B.F. Bai, M.L. Zhong, H.J. Zhang, J.Y. Long, J.P. Han, W.Q. Wang, G.F. Jin, General strategy toward dual-scale-controlled metallic micro-nano hybrid structures with ultralow reflectance, ACS Nano 11 (2017) 7401–7408.

**36.** C.L. Liu, W. Zhou, J.K. Song, H.J. Liu, J.H. Qu, L. Guo, G.F. Song, C.P. Huang, Nanostructure-induced colored TiO2 array photoelectrodes with full solar spectrum harvesting, J. Mater. Chem. A 5 (2017) 3145–3151.

**37.** X.M. Zhong, D.L. Yu, Y. Song, D.D. Li, H.P. Xiao, C.Y. Yang, L.F. Lu, W.H. Ma, X.F. Zhu, Fabrication of large diameter TiO2 nanotubes for improved photoelectrochemical performance, Mater. Res. Bull. 60 (2014) 348–352.

**38.** H. Cheshideh, F. Nasirpouri, Cyclic voltammetry deposition of nickel nanoparticles on TiO2 nanotubes and their enhanced properties for electro-oxidation of methanol, J. Electroanal. Chem. 797 (2017) 121–133.

**39.** J.A. Díaz-Real, E.O. Ortega, M.P. Gurrola, J.L. Garcia, L.G. Arriaga, Light-harvesting Ni/TiO2 nanotubes as photo-electrocatalyst for alcohol oxidation in alkaline media, Electrochim. Acta 206 (2016) 388–399.

**40.** J. Lee, J. Yang, S.G. Kwon, T. Hyeon, Nonclassical nucleation and growth of inorganic nanoparticles, Nat. Rev. Mater. 1 (2016) 16034.

**41.** P. Li, J. Liu, N. Nag, P.A. Crozier, Dynamic nucleation and growth of Ni nanoparticles on high-surface area titania, Sur. Sci. 600 (2006) 693–702.

**42.** J. Ni, K. Noh, C.J. Frandsen, S.D. Kong, G. He, T.T. Tang, S. Jin, Preparation of near micrometer-sized TiO2 nanotube arrays by high voltage anodization, Mater. Sci. Eng. C 33 (2013) 259–264.

**43.** X.H. Gao, Z.M. Guo, Q.F. Geng, P.J. Ma, A.Q. Wang, G. Liu, Microstructure, chromaticity and thermal stability of SS/TiC-WC/Al2O3 spectrally selective solar absorbers,Sol. Energy Mater. Sol. Cells 164 (2017) 63–69.

**44.** D. Venieri, I. Gounaki, V. Binas, A. Zachopoulos, G. Kiriakidis, D. Mantzavinos, Inactivation of MS2 coliphage in sewage by solar photocatalysis using metal-doped TiO2, Appl. Catal. B: Environ. 178 (2014) 54–64.